



HAL
open science

Manipulating the ferroelectric polarization state of BaTiO₃ thin films

Sukanya Datta, Maxime Rioult, Dana Stanescu, H el ene Magnan, Antoine
Barbier

► **To cite this version:**

Sukanya Datta, Maxime Rioult, Dana Stanescu, H el ene Magnan, Antoine Barbier. Manipulating the ferroelectric polarization state of BaTiO₃ thin films. *Thin Solid Films*, 2016, 607, pp.7. 10.1016/j.tsf.2016.03.059 . cea-01369284

HAL Id: cea-01369284

<https://cea.hal.science/cea-01369284>

Submitted on 20 Sep 2016

HAL is a multi-disciplinary open access archive for the deposit and dissemination of scientific research documents, whether they are published or not. The documents may come from teaching and research institutions in France or abroad, or from public or private research centers.

L'archive ouverte pluridisciplinaire **HAL**, est destin ee au d ep ot et  a la diffusion de documents scientifiques de niveau recherche, publi es ou non,  emanant des  tablissements d'enseignement et de recherche fran ais ou  trangers, des laboratoires publics ou priv es.



Manipulating the ferroelectric polarization state of BaTiO₃ thin films



S. Datta, M. Rioult, D. Stanescu, H. Magnan, A. Barbier *

Service de Physique de l'Etat Condensé, SPEC, CEA, CNRS, Université Paris-Saclay, CEA Saclay, 91191 Gif-sur-Yvette Cedex, France

ARTICLE INFO

Article history:

Received 14 October 2015
 Received in revised form 8 March 2016
 Accepted 29 March 2016
 Available online 31 March 2016

Keywords:

Ferroelectric thin films
 Macroscopic polarization
 Microscopic polarization
 Atomic oxygen molecular beam epitaxial method (AO-MBE)
 Piezo response and atomic force microscopy (PFM and AFM)
 Annealing
 Overcurrent

ABSTRACT

Controlling the ferroelectric polarization at macroscopic or microscopic levels is crucial in the framework of the development of ferroelectric materials used in yet challenging photo-electrochemical (PEC) cells and spintronic applications. We report here on polarization methods allowing to electrically polarize prototypical samples of BaTiO₃ (001) films. Epitaxial single crystalline layers were grown up to a thickness of 25 nm by atomic oxygen assisted molecular beam epitaxy on 1 at.% Nb doped SrTiO₃ (001) single crystals. The samples were both microscopically and macroscopically polarized using Piezoresponse Force Microscopy and electrochemical poling in an electrolyte respectively. In addition we demonstrate the possibility to retrieve a quasi-native mixed ferroelectric polarization state after annealing. These polarization methods may be applied to many other ferroelectric thin films.

© 2016 Elsevier B.V. All rights reserved.

1. Introduction

There is currently a strong interest towards developing ferroelectric materials for various applications such as their use in multiferroics systems [1–4], photoelectrochemical cells (PEC) [5–8], and heat and gas sensors [9–11]. Ferroelectricity is a particular property of non-centrosymmetric materials exhibiting a spontaneous electrical polarization that can be reversed by the application of an external electric field. In the recent years, an impressive amount of contributions have focused on the ferroelectric properties of perovskite-based oxides such as BiFeO₃, BaTiO₃, PZT (Lead Zirconium Titanate) [12–17]. For such crystals, in the ferroelectric state, the barycenter of cations and anions in the unit cell are slightly spatially separated, inducing an electric dipole, *i.e.* an electric polarization. Dipoles rearrange themselves to minimize the sample energy forming different ferroelectric domains wherein the electric polarization points towards a given direction. Usually in an as-grown thin ferroelectric film the polarization is not uniform and the sample exhibits several ferroelectric domains where the polarization vector is pointing towards different directions. However, it is possible to control the orientation of the domains through the application of a saturating external electric field that allows the majority of the electrical dipoles within a domain to be oriented in a particular direction. Because of the wealth of technologically important applications deriving from the inclusion of ferroelectric layers in smart devices, it is of major

importance to understand and master the manipulation of the domains electric polarization orientation in thin films, at the microscopic and macroscopic scales. Recently multiferroic BiFeO₃ samples were considered within this framework. M. Singh et al. have reported on the local polarization of BiFeO₃ samples at the microscopic scale by applying a 10 V potential on an AFM tip [18]. Cao et al. have independently demonstrated the poling of BiFeO₃ samples at the macroscopic scale in a solution of Lithium Chlorate (LiClO₄) in propylene carbonate [19]. In the present work we consider the prototypical ferroelectric material BaTiO₃ that has the major advantages as exhibiting a simple perovskite crystalline structure and featuring a para- to ferro-electric transition at relatively high temperature (130 °C for bulk BaTiO₃ and even much higher for strained layers [20]). Here we demonstrate routes to master the manipulation of the polarization state at microscopic and macroscopic scales of BaTiO₃/Nb:SrTiO₃ samples, as well as the possibility to erase an applied polarization state by an air annealing of the very same samples.

2. Experimental details

The BaTiO₃ epitaxial layers were deposited on single crystalline 1 at.% Nb:SrTiO₃ (001) (*i.e.* ~0.5 wt% Nb) substrates using atomic oxygen assisted molecular beam epitaxy (AO-MBE), a technique that makes possible the deposition of single crystalline layers of controlled morphology, stoichiometry and thickness [21]. The doped substrate is conductive enough to use it as electrode during the BaTiO₃ overlayer poling procedures. The oxide layers were formed by thermal

* Corresponding author.
 E-mail address: antoine.barbier@cea.fr (A. Barbier).

evaporating high purity metals from Knudsen cells, while exposing the sample to an atomic oxygen plasma (RF power = 350 W) in an ultra-high vacuum vessel (10^{-7} mbar working conditions, 10^{-10} mbar base pressure). In order to have a homogeneous deposition and to reach the expected stoichiometry, the samples are rotated continuously around their surface normal during the deposition while kept at a temperature of ~ 900 K. The oxide deposition rate was about 0.12 nm/min. To investigate the quality and the structure of the grown epitaxial films, *in situ* reflection high-energy electron diffraction (RHEED) patterns were acquired during the film growth. The thickness of the BaTiO₃ layers investigated in the present work lies in-between 15 and 30 nm. In this range no influence of thickness on any measurements could be observed within the techniques used in this paper which is noticeably consistent with the previous report by Kim et al. [22] who reported a critical thickness for ferroelectricity of BaTiO₃ of 4 nm and very little changes of the remnant polarization with thickness above 15 nm.

In situ XPS spectra of the Ba 3d, Ti 2p and O 1s core levels, using Al-K α radiation, were systematically recorded just after deposition to check the consistency of the BaTiO₃ layer stoichiometry with previous reports [21]. XPS spectra were also recorded after the different polarization treatments to check eventual compositional changes in the layers.

We used Atomic Force Microscopy (AFM) and Piezoresponse Force Microscopy (PFM) to investigate the surface morphology and ferroelectric properties of our samples respectively. The images were realized with a Brüker™ scanning probe microscope and a Nanoscope V controller.

The samples were electrically poled using two major strategies as depicted schematically in Fig. 1. (i) *Local poling* (microscopic scale) was achieved using PFM, which was used in writing mode to create well defined ferroelectric domains in our samples, by poling with various positive or negative potentials applied on the tip (in the [0 V, 10 V] range), Fig. 1a and b. Since, the back of the sample was always connected to the ground, the sample surface was thus exposed to potentials in the [−10 V, +10 V] range. This poling procedure will be hereafter referred to as PFM-poling. The tip velocity was 0.4 $\mu\text{m/s}$ and the writing resolution was 20 nm. (ii) *Macroscopic poling* was realized using a non-aqueous LiClO₄ electrolyte (0.1 M LiClO₄ in propylene carbonate), with a large electrochemical window (*i.e.* a large voltage range in between which the substance is neither oxidized nor reduced), in an electrochemical cell with 2 electrodes. The sample was mounted as the working electrode and a Pt wire as the counter electrode. The geometry of the experimental setup is shown on Fig. 1c and d and a scheme of the experiment is given on Fig. 1e. This poling procedure will be hereafter referred to as EC-poling. During the EC-poling procedure, the sample was kept at 0 V. Potentials of +8 V and −8 V were applied several times alternatively (while monitoring the current) on the platinum counter electrode (during 10 s each) in order to reinforce the ferroelectric state as proposed by Roelofs et al. [23]. To obtain a remnant electric polarization pointing towards the substrate (by convention called downward polarization), the last applied potential was +8 V. Indeed,

in a previous work [5], we demonstrated that +8 V EC-poling leads to downward polarization of the BaTiO₃ layer. Lastly the electric current monitoring is of crucial importance during EC-poling since overcurrent appeared to be strongly detrimental to the samples as we will demonstrate later in this paper.

The PFM-poled written ferroelectric domains were observed by PFM and Low Energy Electron Microscopy (LEEM). Beyond the recognized full field morphology characterization capabilities of LEEM [24,25], it has been previously reported that surface charge changes, expected when the ferroelectric polarization orientation changes, provide a visible LEEM contrast [26]. This phenomenon was used to observe ferroelectric contrasts between polarized and unpolarized regions of the sample regions. The samples were optically patterned by laser lithography and e-beam evaporation to include metallic Au landmarks on the sample surface that allow finding the PFM polarized regions easily. The 200 nm thick Au landmarks were evaporated on top of a 15 nm thick Ti seed layer. For a broader view, one may also use Kelvin probe force microscopy [27,28] or scanning surface potential microscopy [29] to map the surface charge changes due to different ferroelectric domains polarization orientations, and DARTSPFM for P–E loops measurements [30].

The high chemical stability in air of BaTiO₃, as well as of the Nb:SrTiO₃ substrates, allows for air annealing at high temperature without composition changes. Since annealing above the ferroelectric order-disorder temperature is easily possible in air, it appears as a method of choice to “reset” the ferroelectric domains orientation after PFM- or EC-poling. This was realized in a high temperature furnace above the Curie temperature of BaTiO₃ with typical rates of 14 °C/min up to 280 °C.

3. Results and discussion

3.1. Growth

In situ RHEED patterns were observed and acquired during film growth to monitor the quality and the structure of the grown epitaxial samples. Upon growth, the RHEED patterns switched from features typical of the perovskite Nb:SrTiO₃ substrate to the ones characteristic of the BaTiO₃ thin epitaxial film (Fig. 2), similarly to observations reported using undoped SrTiO₃ (001) substrates [21]. By convention we indexed the reciprocal space using the reciprocal space unit vectors (10)* and (01)* to describe the primitive reciprocal surface lattice as depicted in Fig. 2e. The RHEED reciprocal space streaks remain mostly 2D rod-like with some hints of island formation for high thicknesses (intensity modulations along the streaks at high thickness). The surface lattice parameter can easily be extracted from the streaks position while the error bar is derived from the parameter dispersion obtained using several azimuths. The surface lattice parameter evolution (Fig. 2f) reveals an almost complete structural relaxation for thicknesses above 10 nm. From our RHEED observations we can conclude that the layers are mainly epitaxial, single crystalline and flat.

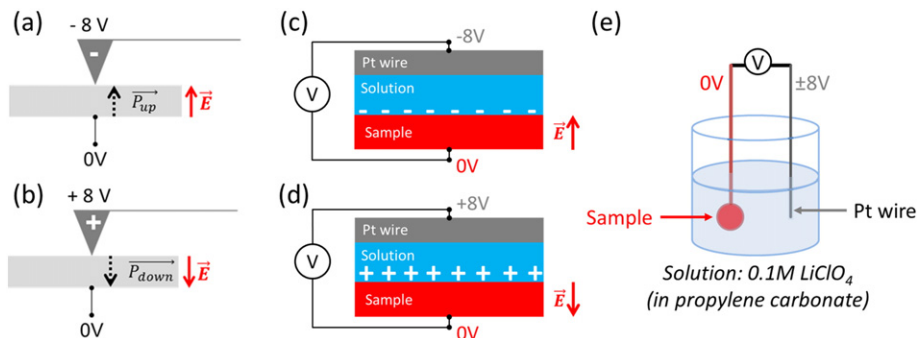


Fig. 1. (a) to (d) Geometry and expected polarization states using PFM-poling with −8 V (a) and +8 V (b) poling potentials and using EC-poling with −8 V (c) and +8 V (d) poling potentials. (e) Scheme of the EC-poling experiment.

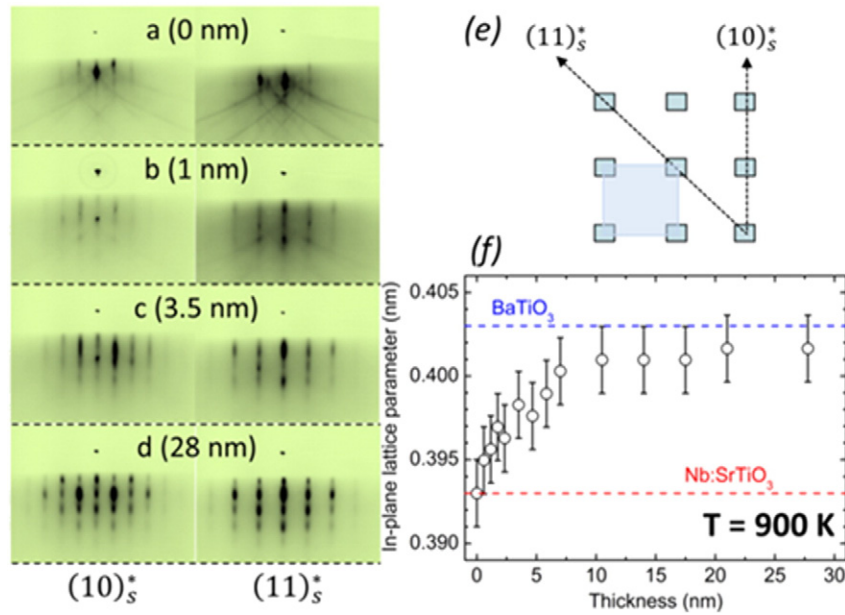


Fig. 2. (Left panel) RHEED patterns of a 28 nm BaTiO₃ film grown by AO-MBE on Nb:SrTiO₃ at different deposition times/thicknesses (steps (a) to (d)) over the two lowest Miller index surface diffraction directions. (e) The corresponding surface reciprocal lattice is represented; making explicit the diffraction directions, the elementary cell (in the reciprocal space) is also shown. (f) In-plane lattice parameter derived from the RHEED data with the same method as in reference [21]. Dashed lines stand for the in-plane lattice parameter of bulk BaTiO₃ (blue-top) and Nb:SrTiO₃ (red-bottom) at the deposition temperature of 900 K (taking into account the thermal expansion).

The chemical composition of the as-grown layers was investigated by *in situ* XPS. A wide scan recorded over the entire accessible binding energy region (Fig. 3) shows the presence of the expected species (Ti, O and Ba) and no additional eventual surface contamination. As previously reported in reference [21] a Ba rich surface oxide is necessary to promote a good epitaxial growth leading to Ba/Ti ratio above unity (typically ~1.3). The binding energy of the Ba 3d^{5/2} line was found at 780.4 eV from detailed measurements of the Ba 3d XPS lines as reported in Fig. 4.

3.2. Microscopic polarization

The ferroelectric nature of the layers was investigated by PFM. Scanning the tip-surface potential in the [−10 V, +10 V] range evidences two distinct polarization states. In order to determine the ferroelectric domain repartition we locally polarized the sample by applying +8 V

and −8 V on the tip (substrate at ground) accordingly to the pattern shown in Fig. 5a. After the PFM-poling the pattern was read again by PFM using a sinusoidal potential applied on the sample (tip at ground) with a drive amplitude of 4000 mV. The resulting PFM phase image is shown in Fig. 5b. The integrated phase profile through the image of the written pattern (Fig. 5c) shows 3 different phase levels (58°, −60° and 54°) corresponding to the different remnant states: (i) +8 V PFM-poled, (ii) −8 V PFM-poled and (iii) outside the writing region (*i.e.* 0 V or ‘as-grown’), respectively. One may note that in this case the PFM phase of the as-grown region (54°) is close to the one after +8 V polarization (58°). This result shows that the as-grown state behaves more like the +8 V polarization states rather than like the −8 V ones and that the ferroelectric domain mix between *up* and *down* orientations is different in each region. Moreover we observe that the PFM phase difference between the +8 V and −8 V remnant states is about 118°, which is smaller than the expected 180° value. This phenomenon has been examined in more details in previous reports and can have

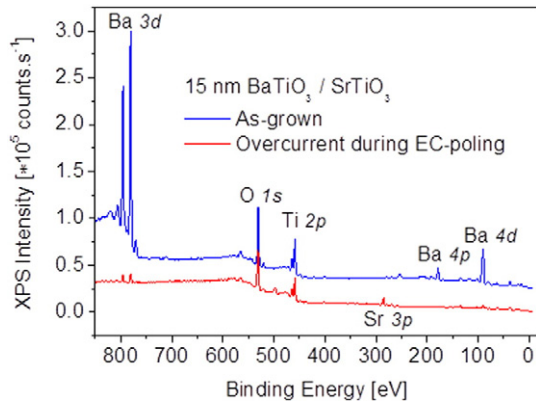


Fig. 3. Wide XPS scan of a 15 nm thick BaTiO₃/Nb:SrTiO₃ (001) sample elaborated by AO-MBE. ((blue, top curve) As grown sample and (red, bottom curve) for the same sample having experienced overcurrent during the macroscopic EC-poling procedure. The O 1s line (located at ca. 530.1 eV) of the as-grown sample was used as a reference position and the curves were shifted vertically for the sake of clarity.

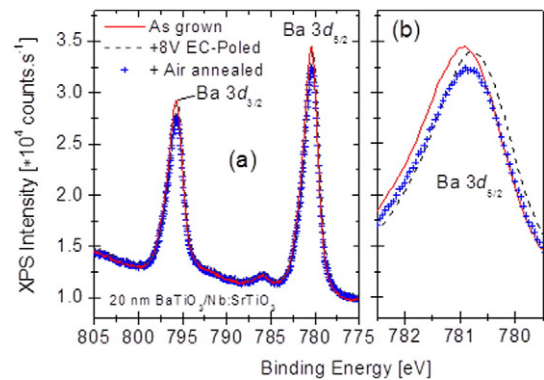


Fig. 4. Ba 3d XPS photoemission lines (a) recorded for a 20 nm BaTiO₃/Nb:SrTiO₃ (001) layer grown by AO-MBE and (b) enlarged region of the main Ba 3d_{5/2} line: (—, red solid line) as-grown layer, (---, black dashed line) after +8 V EC-poling in a LiClO₄ bath and (+, blue cross-plus) after +8 V EC-poling and a subsequent annealing in air at 280 °C.

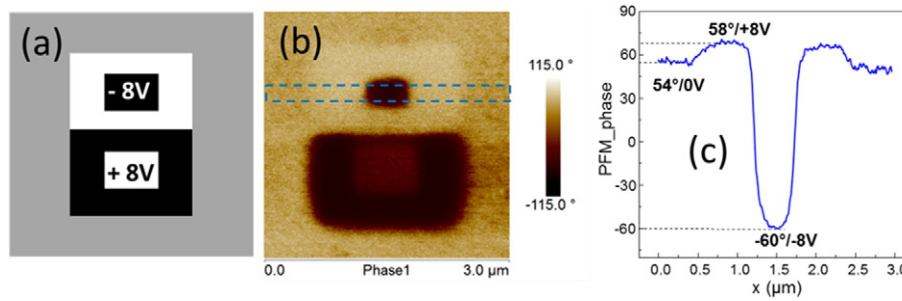


Fig. 5. PFM measurements performed on a 15 nm thick BaTiO₃/Nb:SrTiO₃(001) sample realized by AO-MBE. (a) Sketch of the written pattern used to locally polarize the sample; (b) observed PFM phase pattern in reading mode after writing at ± 8 V the pattern as described in (a) and using a drive amplitude of 4000 mV; (c) integrated intensity along the blue dashed box depicted in (b).

different origins: (i) the domains are not fully polarized (*i.e.* a mix of upward and downward domains); (ii) the PFM signal is disturbed by a background signal [31] inherent to the PFM setup; (iii) an asymmetry in polarization orientation may arise from an internal built-in electric field at the bottom interface which may result in incomplete 180° switching [32]; and/or the drive amplitude was large enough to induce a charge build-up. Although the later effect is unlikely since successive scans did not evidenced any evolution of the patterns. However, one may note that an improved contrast using lower drive amplitude may be obtained thanks to the DARTSSPFM method [30], unfortunately this mode was not available in our setup. From region to region or sample to sample (within a set of about 10 samples) the observed domain mix, in the as-grown region, spans a wide range from nearly equiprobable to almost single domain. We can thus conclude that for the as-grown samples, the ferroelectric domains are arranged in a random fashion, *i.e.* a mix of upward and downward states.

PFM written patterns were subsequently investigated using full field LEEM imaging. Contrarily to PFM that can be used for writing and reading patterns, the LEEM technique allows a rapid investigation of large areas of the sample without eventual unwanted modifications as could be induced by a scanning tip, like during PFM measurements. Prior to LEEM imaging the sample was outgassed for several hours at 80 °C. Working close to the Mirror Electron Microscopy (MEM) to LEEM transition (starting voltage close to 1 V) allows the best imaging conditions and contrast. Thanks to the Au landmarks, the written pattern can easily be located as it can be seen in Fig. 6b (50 μ m field of view (FOV)). A closer inspection with a FOV of 10 μ m (Fig. 6c) confirms the presence of 3 different contrasts and thus the mixed initial polarization states of the as-grown samples. The LEEM observations are fully consistent with the previous PFM analysis.

3.3. Macroscopic polarization

After a PFM-poling (using the pattern shown on Fig. 6a), the sample was macroscopically EC-poled by keeping the current below 1 mA and observed again by LEEM. As it can be seen in Fig. 6d the pattern completely vanished upon this +8 V EC-poling procedure, indicating

that the macroscopic polarization overcomes the PFM writing. To confirm that the ferroelectric properties of the sample were unaltered by the EC-poling we performed again a PFM-poling using the initial PFM pattern in identical conditions and observed it subsequently by LEEM. As it can be seen in Fig. 6e the pattern is clearly visible defining again 3 contrasts states (+8 V remnant state, -8 V remnant state and EC-poled remnant states). In addition one may note that the surface morphology does not evolve upon EC-poling, remaining smooth and flat. Moreover, as revealed by XPS the composition remained unchanged after EC-poling since the peak intensities only marginally varied (Fig. 4). The peak position of the Ba 3d^{5/2} line (Fig. 4b) is shifted to 780.2 eV. This shift is likely linked to a global surface charge effect although it is only slightly above the experimental error bar. Therefore we can conclude that EC-poling a BaTiO₃ epitaxial layer in LiClO₄ while keeping the current below 1 mA during the poling procedure changes neither the surface composition nor the morphology of the sample.

3.4. Overcurrent

By studying EC-poling with different successive increasing currents flowing through the sample, we found out that a current flow above 1 mA leads to detrimental results. We investigated in more details the effect of not limiting the current flowing through the sample during the EC-poling procedure. AFM images of a sample having experienced EC-poling without limiting the current (overcurrent) is reported in Fig. 7. During the EC-poling procedure, the sample was mounted in a special sample holder and fixed with a sealing joint in order to avoid the electrolyte to be in contact to the back of the substrate. As a matter of fact, the macroscopic polarization of the samples required some particular attention. Since BaTiO₃ is ferroelectric and in consequence necessarily also piezoelectric, a mechanical strain may compete or even overcome the effect of an external electric field when one desires to tune the internal ferroelectric polarization. It is thus mandatory to get rid of any mechanical strain while performing an external poling procedure. In the case of our EC-poling procedure this was achieved by etching out a ring down to the substrate on the sample that corresponds to

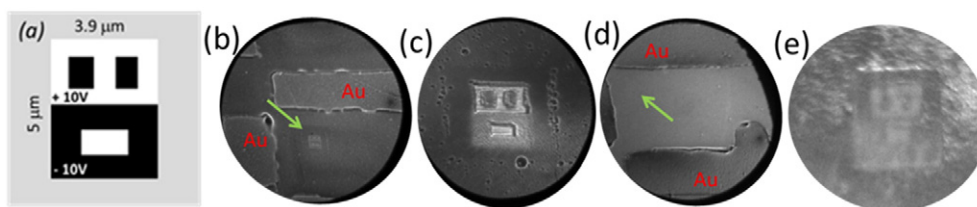


Fig. 6. LEEM images of a 15 nm thick BaTiO₃/Nb:SrTiO₃(001) sample elaborated by AO-MBE. (a) PFM pattern used to write ferroelectric domains using ± 10 V electric potentials; (b) and (c) as grown situation with written PFM pattern for two field of views (FOV) (50 μ m and 10 μ m respectively) – The rectangular features are Au landmarks, as indicated – the arrow in (b) highlights the ease of observation of a the written pattern with respect to the landmarks. (d) Observation of the same region (50 μ m FOV) than (a) after macroscopic EC-poling of the sample with a potential of +8 V in LiClO₄, the arrow indicates the original position of the PFM pattern; (e) observation of the same region than (d) (10 μ m FOV) after writing again the PFM pattern depicted in (a) after EC-poling (10 μ m FOV). All images were taken around the MEM-LEEM transition potential with starting voltages ranging from 0.8 to 1.2 V.

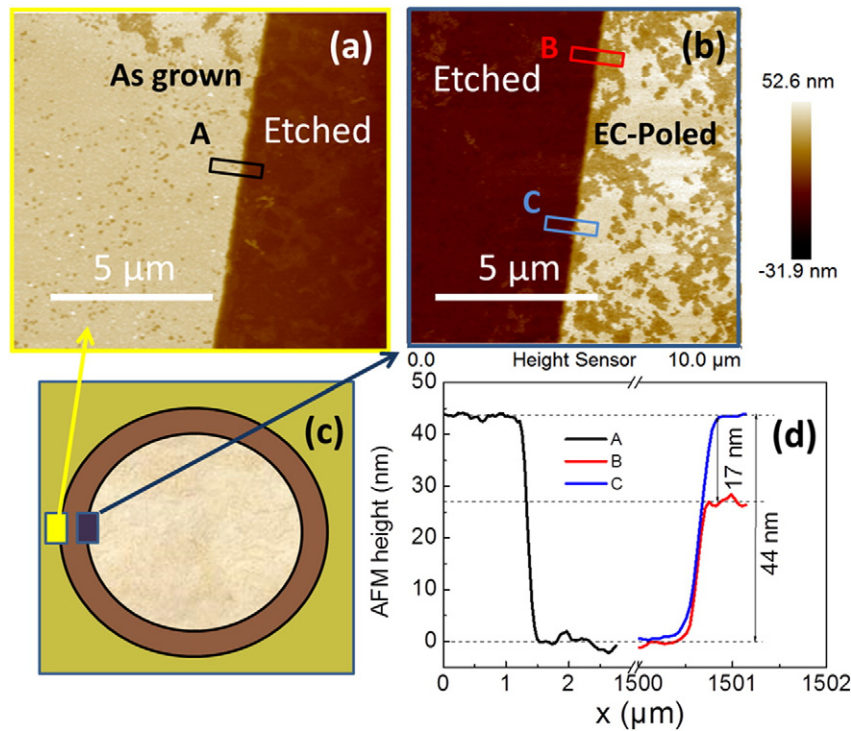


Fig. 7. Fast Scan AFM images recorded on a 30 nm thick BaTiO₃/Nb:SrTiO₃ (001) sample elaborated by AO-MBE on both sides of an etched ring after the sample having been exposed to an overcurrent during the macroscopic EC-polling polarization in LiClO₄. (a) Region non-exposed to the electrolyte (no overcurrent, unpolarized as-grown, left region) and a fraction of the ring (right region); (b) fraction of the ring (left region) and region exposed to the electrolyte (EC-poled, overcurrent, right region); (c) schematic drawing of the sample with the etched ring and (d) integrated step heights as measured on zones labeled A, B and C in (a) and (b).

the position of the electrochemical cell sealing joint (Fig. 7). The etched ring for sealing purpose separates the sample in two regions: outside the ring the 30 nm thick BaTiO₃ layer was not exposed to the electrolyte (Fig. 7a) while the inside region which was EC-poled in LiClO₄ was the siege of eventual overcurrent situations (Fig. 7b). This ring patterning allows comparing, on the same BaTiO₃ sample, surfaces which underwent overcurrent upon EC-poling (Fig. 7b, inside) or not (Fig. 7a, outside). Integrated topography profiles at locations corresponding to different contrasts (Fig. 7d) show that the difference of height between the B and C regions is around 17 nm. Since the nominal thickness of this BaTiO₃ film was 30 nm, we can conclude that the darker regions correspond to sample zones where the BaTiO₃ film partially disappeared. The film morphology and thickness seem unperturbed in the lighter (unexposed) regions. The corresponding global XPS scan (Fig. 3) recorded on this sample confirms the massive loss of BaTiO₃ after the overcurrent exposure of the surface, which is most likely due to the dissolution in the electrolyte.

3.5. Annealing

Macroscopic single polarization states as likely produced by EC-poling may be interesting for specific applications. For example we could show a 2.5 times increased photocurrent density during solar water splitting using a polarized BaTiO₃ layer with respect to a non-polarized configuration [5]. However, for many aspects, it is very desirable to be able to reset the sample domain configuration. To ensure the complete control of the ferroelectric polarization and the repeatability of our different poling procedures, we performed an air annealing of an EC-poled samples at 280 °C (above the Curie temperature of BaTiO₃). After annealing we could write again patterns using PFM indicating that after crossing the Curie temperature the sample came back to a more mixed polarization state (effective ferroelectric polarization “reset”). XPS showed unchanged composition and the Ba 3d^{5/2} lines were found at a position intermediate between the as-grown situation

and the EC-poled ones (Fig. 4b). The ability to reset the polarization state was investigated in more details by PFM starting from a virgin sample. The ferroelectric domain configuration of a 15 nm thick BaTiO₃/Nb:SrTiO₃ layer was investigated before and after annealing in air at 280 °C for 20 min (Fig. 8). The sample possessed Au landmarks, realized by lithography, to allow a precise positioning of the tip on a given region that was observed prior (Fig. 8a) and after writing (Fig. 8b). The very same region was imaged again after a sample annealing realized at 280 °C for 20 min. As can be seen on Fig. 8c the pattern was “erased” after the annealing procedure. Finally, we checked that the sample showed similar ferroelectric behavior after annealing by writing a pattern on another region of the same sample, as observed in Fig. 8d. From these observations we can conclude that after an annealing cycle the ferroelectric configuration of the layer is “reset” to a new mixed polarization state configuration.

4. Conclusion

In conclusion, we have demonstrated efficient methods to manipulate the polarization state of a prototypical BaTiO₃ ferroelectric layer and also to retrieve a new mixed polarization state after macroscopic polarization. We showed that our layers can be locally polarized using PFM within the [−10 V; +10 V] potential range. We have also shown that the BaTiO₃ layer can be downward polarized macroscopically in a solution of LiClO₄ in propylene carbonate chloride, provided that the current is maintained below 1 mA. Upon overcurrent the BaTiO₃ layer is likely to dissolve. Moreover, we found that an air annealing at a temperature above the Curie temperature performs a sort of “reset” of the ferroelectric polarization. Our study presented a set of tools in order to master the polarization states of ferroelectric layers, which is of top interest in the framework of the use of ferroelectric materials in new devices having tremendous potential in many technologically important fields like multiferroics for spintronics or photoelectrochemical water splitting devices in particular.

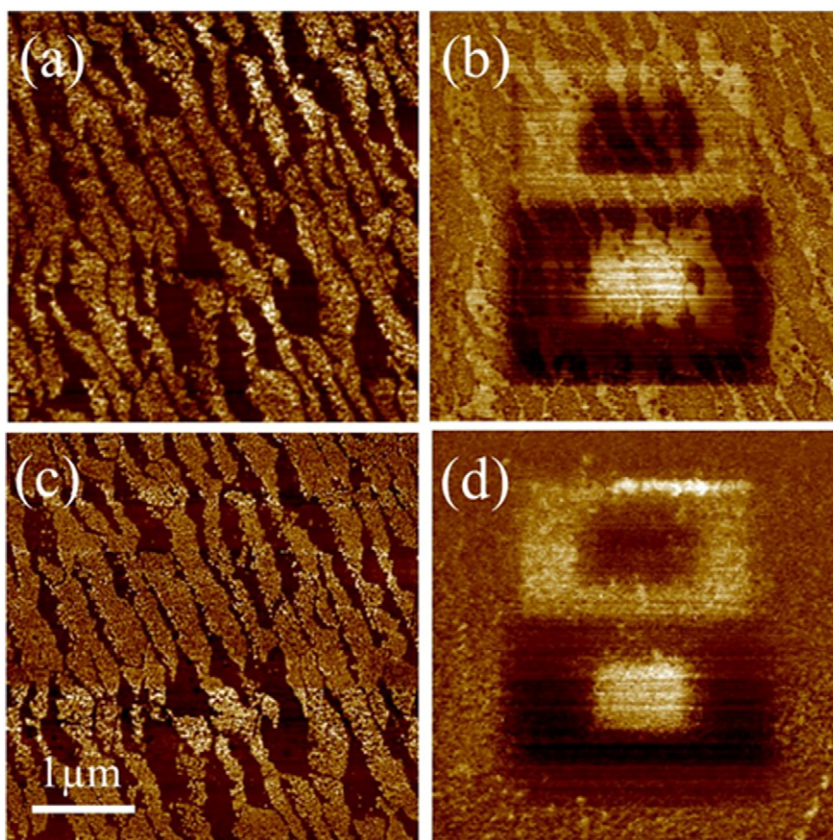


Fig. 8. PFM measurements on a 15 nm thick BaTiO₃/Nb:SrTiO₃(001) sample realized by AO-MBE for (a) the as grown sample; (b) after writing at ± 8 V the pattern as described in Fig. 5a; (c) same region than (b) observed after a sample annealing at 280 °C for 20 min and (d) after writing again the pattern on the sample on a virgin region.

Conflict of interest

The authors declare no conflict of interest.

Acknowledgements

This work was funded by the CEA (DSM-Energie program under the PAPI grant) and supported in part by Triangle de la Physique and Ile-de-France (C'Nano and ISC-PIF) under the IMAMFP grants.

References

- [1] Y. Tokunaga, N. Furukawa, H. Sakai, Y. Taguchi, T.-H. Arima, Y. Tokura, Composite domain walls in a multiferroic perovskite ferrite, *Nat. Mater.* 8 (2009) 558.
- [2] Evgeny Y. Tsybmal, Elbio R.A. Dagotto, Chang-Beom Eom, Ramamoorthy Ramesh, Multifunctional Oxide Heterostructures, OUP Oxford, 2012 ISBN: 9780199584123.
- [3] N. Jedrecy, H.J. von Bardeleben, V. Badjeck, D. Demaille, D. Stanesco, H. Magnan, A. Barbier, Strong magnetoelectric coupling in multiferroic Co/BaTiO₃ thin films, *Phys. Rev. B* 88 (2013) 121409(R).
- [4] A. Barbier, T. Aghavonian, V. Badjeck, C. Mocuta, D. Stanesco, H. Magnan, C.L. Rountree, R. Belkhou, P. Ohresser, N. Jedrecy, Antiferromagnetic long-range spin ordering in Fe- and NiFe₂-doped BaTiO₃ multiferroic layers, *Phys. Rev. B* 91 (2015) 035417.
- [5] M. Rioult, S. Datta, D. Stanesco, S. Stanesco, R. Belkhou, F. Maccherozzi, H. Magnan, A. Barbier, Tailoring the photocurrent in BaTiO₃/Nb:SrTiO₃ photoanodes by controlled ferroelectric polarization, *Appl. Phys. Lett.* 107 (2015) 103901.
- [6] W. Ji, K. Yao, Y.F. Lim, Y.C. Liang, A. Suwardi, Epitaxial ferroelectric BiFeO₃ thin films for assisted photocatalytic water splitting, *Appl. Phys. Lett.* 103 (2013) 062901.
- [7] K. Meng, P.K. Suroolia, K.R. Thampi, BaTiO₃ photoelectrodes for CdS quantum dot sensitized solar cells, *J. Mater. Chem. A* 2 (2014) 10231.
- [8] S. Park, C.W. Lee, M.-G. Kang, S. Kim, H.J. Kim, J.E. Kwon, S.Y. Park, C.-Y. Kang, K.S. Hong, K.T. Nam, A ferroelectric photocatalyst for enhancing hydrogen evolution: polarized particulate suspension, *Phys. Chem. Chem. Phys.* 16 (2014) 10408.
- [9] G. Dong, H. Fan, H. Tian, J. Fang, Q. Li, Gas-sensing and electrical properties of perovskite structure p-type barium-substituted bismuth ferrite, *RSC Adv.* 5 (2015) 29618.
- [10] A. Navrotsky, Thermochemistry of perovskite-related oxides with high oxidation states: superconductors, sensors, fuel cell materials, *Pure Appl. Chem.* 66 (1994) 1759.
- [11] T. Tasaki, S. Takase, Y. Shimizu, Fabrication of Sm-based perovskite-type oxide thin-films and gas sensing properties to acetylene, *J. Sens. Technol.* 2 (2012) 75.
- [12] K.Y. Yun, D. Ricinchi, T. Kanashima, M. Noda, M. Okuyama, Giant ferroelectric polarization beyond 150 $\mu\text{C}/\text{cm}^2$ in BiFeO₃ thin film, *Jap. J. Appl. Phys.* 43 (2004) L647.
- [13] S.Y. Yang, F. Zavaliche, L. Mohaddes-Ardabili, V. Vaithyanathan, D.G. Schlom, Y.J. Lee, Y.H. Chu, M.P. Cruz, Q. Zhan, T. Zhao, R. Ramesh, Metalorganic chemical vapor deposition of lead-free ferroelectric BiFeO₃ films for memory applications, *Appl. Phys. Lett.* 87 (2005) 102903.
- [14] K. Iijima, T. Terashima, K. Yamamoto, K. Hirata, Y. Bando, Preparation of ferroelectric BaTiO₃ thin films by activated reactive evaporation, *Appl. Phys. Lett.* 56 (1990) 527.
- [15] K.S. Young, K.S. Kim, Y.D. Park, J.-G. Yoon, Critical thickness of ultrathin ferroelectric BaTiO₃ films, *Appl. Phys. Lett.* 86 (2005) 102907.
- [16] J. Fukushima, K. Kodaira, T. Matsushita, Preparation of ferroelectric PZT films by thermal decomposition of organometallic compounds, *J. Mater. Sci.* 19 (1984) 595.
- [17] R. Moazzami, C. Hu, W.H. Shepherd, Electrical characteristics of ferroelectric PZT thin films for DRAM applications, *IEEE Trans. Electron Devices* 39 (1992) 9.
- [18] M. Singh, Y. Yang, C.G. Takoudis, A. Tatarenko, G. Srinivasan, P. Kharel, G. Lawes, Metallorganic chemical-vapor-deposited BiFeO₃ films for tunable high-frequency devices, *Electrochem. Solid-State Lett.* 12 (2009) H161.
- [19] D. Cao, Z. Wang, L. Nasori, Y. Wen, Mi, Y. Lei, Switchable charge-transfer in the photoelectrochemical energy-conversion process of ferroelectric BiFeO₃ photoelectrodes, *Angew. Chem.* 126 (2014) 11027.
- [20] K.J. Choi, M. Bieganski, Y.L. Li, A. Sharan, J. Schubert, R. Uecker, P. Reiche, Y.B. Chen, X.Q. Pan, V. Gopalan, L.-Q. Chen, D.G. Schlom, C.B. Eom, Enhancement of ferroelectricity in strained BaTiO₃ thin films, *Science* 306 (2014) 1005.
- [21] A. Barbier, C. Mocuta, D. Stanesco, P. Jegou, N. Jedrecy, H. Magnan, Surface composition of BaTiO₃/SrTiO₃(001) films grown by atomic oxygen plasma assisted molecular beam epitaxy, *J. Appl. Phys.* 112 (2012) 114116.
- [22] Y.S. Kim, D.H. Kim, J.D. Kim, Y.J. Chang, T.W. Noh, J.H. Kong, K. Char, Y.D. Park, S.D. Bu, J.-G. Yoon, J.-S. Chung, Critical thickness of ultrathin ferroelectric BaTiO₃ films, *Appl. Phys. Lett.* 86 (2005) 102907.
- [23] Andreas Karl Roelofs, Martin Gerard Forrester and Joachim Walter, US patent US 2007/0041233 A1 (2007).
- [24] E. Bauer, Low energy electron microscopy, *Rep. Prog. Phys.* 57 (2014) 895–938 (R).
- [25] E. Bauer, Low-Energy Electron Microscopy, in: G. van Tandeloo, Dirk Van Dyck, S.J. Pennycook (Eds.), *Handbook of Nanoscopy*, Wiley 2012, pp. 673–696 (R).

- [26] J.E. Rault, W. Ren, S. Prosandeev, S. Lisenkov, D. Sando, S. Fusil, M. Bibes, A. Barthelemy, L. Bellaiche, N. Barrett, Thickness-dependent polarization of strained BiFeO₃ films with constant tetragonality, *Phys. Rev. Lett.* 109 (2012) 267601.
- [27] Y. Kim, S. Bühlmann, J. Kim, M. Park, K. No, Local surface potential distribution in oriented ferroelectric thin films, *Appl. Phys. Lett.* 91 (2007) 052906.
- [28] L. Wang, K.-J. Jin, J.-X. Gu, C. Ma, X. He, J. Zhang, C. Wang, Y. Feng, Q. wan, J.-A. Shi, M. He, H.-B. Lu, G.-Z. Yang, A new non-destructive readout by using photo-recovered surface potential contrast, *Sci. Rep.* 4 (2014) 6980.
- [29] X.Q. Chen, H. Yamada, T. Horiuchi, K. Matsushige, S. Watanabe, M. Kawai, P.S. Weiss, Surface potential of ferroelectric thin films investigated by scanning probe microscopy, *J. Vac. Sci. Technol. B* 17 (1999) 1930.
- [30] B.J. Rodriguez, C. Callahan, S.V. Kalinin, R. Proksch, Dual-frequency resonance-tracking atomic force microscopy, *Nanotechnology* 18 (2007) 475504.
- [31] T. Jungk, A. Hoffmann, E. Soergel, Quantitative analysis of ferroelectric domain imaging with piezoresponse force microscopy, *Appl. Phys. Lett.* 89 (2006) 163507.
- [32] A. Gruverman, A. Kholkin, A. Kingon, H. Tokumoto, Asymmetric nanoscale switching in ferroelectric thin films by scanning force microscopy, *Appl. Phys. Lett.* 78 (2001) 2751.